This is the post-print, accepted manuscript in *IEEE Transactions on Control Systems Technology*: "Port-Hamiltonian flight control of a fixed-wing aircraft," J.-M. Fahmi and C. A. Woolsey. *IEEE Trans. Control Systems Technology* **30**(1), pp. 408-415, January 2022. [DOI: 10.1109/TCST.2021.3059928]

Port-Hamiltonian Flight Control of a Fixed-Wing Aircraft

Jean-Michel Fahmi*and Craig A. Woolsey†
Virginia Tech, Blacksburg, VA, 24060

Abstract

This paper addresses the problem of stabilizing steady, wings level flight of a fixed-wing aircraft to a specified inertial velocity (speed, course, and climb angle). Target rotational dynamics are designed to minimize control-induced sideslip. The aircraft is modeled as a port-Hamiltonian system and the passivity of this system is leveraged in devising the nonlinear control law. The aerodynamic force model in the port-Hamiltonian formulation is quite general; the static, state feedback control scheme requires only basic assumptions concerning lift, side force, and drag. Following an energy-shaping approach, the static state feedback control law is designed to leverage the open-loop system's port-Hamiltonian structure in order to construct a control Lyapunov function Asymptotic stability of the desired flight condition is guaranteed within a large region of attraction. Simulations comparing the proposed flight controller with conventional linear and nonlinear methods demonstrate its advantages.

1 Introduction

Conventional approaches to flight control of fixed-wing aircraft rely on linearizing the vehicle dynamics about an equilibrium motion, such as wings-level flight at constant altitude and speed, and developing a classical, frequency domain control architecture. State-space control schemes, such as linear quadratic or $\mathcal{H}_\infty$ control, are often used but, like classical controllers, these methods ultimately rely on a small perturbation model, limiting their effectiveness to a neighborhood of the nominal flight condition. One can partially address this issue by developing a family of controllers that are parameterized by the desired speed, climb angle, etc., but the performance and stability of the resulting closed-loop system will generally depend on the rate of parameter variation.

To obtain effective closed-loop performance with stability guarantees over a larger operating envelope, one may instead consider nonlinear control design methods such as dynamic inversion [1–3] or adaptive control [4–6]. Dynamic inversion, or feedback linearization, requires a well-characterized model of the nonlinear dynamics. Such a model may be impractical to obtain over the full flight envelope, particularly for an aircraft whose configuration and inertial parameters vary substantially between flights. Model reference adaptive control and adaptive backstepping can accommodate a variety of uncertainties, including uncertain nonlinearities, assuming the system satisfies certain structural conditions. The resulting dynamic state feedback controllers are often computationally sophisticated, however, which can limit their utility for low-cost platforms such as small unmanned aircraft.

The design proposed in this paper is based on modeling the aircraft as a port-Hamiltonian system (PHS) [7], which extends the concept of Hamiltonian systems in classical mechanics to systems with inputs, outputs,

*Jean-Michel Fahmi is a Ph.D Student in the Crofton Department of Aerospace and Ocean Engineering, Blacksburg, VA 24061 USA (e-mail: fahmi@vt.edu)

†Craig A. Woolsey is with the Crofton Department of Aerospace and Ocean Engineering, Blacksburg, VA 24061 USA (e-mail: cwoolsey@vt.edu)

and dissipative forces. PHS are characterized by a scalar function representing the total energy of the system along with a pair of matrix functions that describe how energy is distributed and dissipated. The inputs and outputs of a PHS act as "ports" through which the system exchanges energy with other external systems. Modeling the system as a PHS facilitates nonlinear, energy-based control design and allows using established energy-shaping techniques for PHS [8], such as interconnection and damping assignment, passivity-based control (IDA-PBC) [9]. Passivity-based control (PBC) has proven to be effective in various applications such as the control of electric motors [10], robots [11], rotary inverted pendulums [12, 13] and quadrotors [14–18].

Of the many mechanical system applications of PBC described in the current literature, perhaps the closest to the proposed application of fixed-wing aircraft flight control is the use of PBC to control unmanned underwater vehicles (UUVs). Woolsey and Techy [19] developed a cross-track control law for a slender, underactuated UUV using potential energy shaping, a component concept in PBC. Fahmi and Woolsey [20] adapted this notion of potential energy shaping for directional stabilization of a fixed-wing aircraft. The closed-loop performance, however, exhibited undesirable excursions in the aerodynamic angles, particularly in sideslip. In a different approach to energy shaping, Valentinis *et al* [21] developed a feedback controller for a slender, underactuated UUV by shaping the target dynamics and suppressing the influence of unactuated degrees of freedom. In [22], Valentinis *et al* expanded the scope of control design to include precision guidance along a helical trajectory. More recently, Valentinis and Woolsey [23] developed a passivity-based controller for a non-neutrally buoyant, underactuated submarine executing an emergency ascent.

With the exception of the last example, the studies mentioned above assumed that the vehicle is neutrally buoyant. While hydrodynamic forces such as lift and drag certainly affect vehicle motion, the nominal state of motion is to advance at constant speed with minimum drag and zero lift. In contrast, fixed-wing aircraft rely on aerodynamic lift to counter the gravitational force in steady flight and to execute maneuvers. The work presented in this paper focuses on stabilizing the aircraft velocity by exploiting some remarkable properties of the aerodynamic force when expressed in a port-Hamiltonian framework. The approach to control design is inspired by the canonical transformation approach proposed by Fujimoto *et al* [24].

The paper is organized as follows. Section 2 describes the structure of a port-Hamiltonian system and summarizes the control design approach of Fujimoto *et al* [24]. Section 3 presents the rigid body model for a fixed-wing aircraft, including a novel representation of the aerodynamic force in the PHS framework. The aerodynamic force model is quite general, so the resulting control strategy is effective for widely varying geometries. Section 4 describes the application of the method presented in Section 2 to the model presented in Section 3. Section 6 gives concluding remarks.

2 Port-Hamiltonian Systems

The trajectory tracking control design method described by Fujimoto *et al* [24], which serves as the basis for the control design presented in this paper, is based on a general theoretical framework for underactuated (electro-)mechanical systems. The approach relates to the IDA-PBC method described by Ortega *et al* [9]; Fujimoto's [24] approach may be interpreted as a variant of the latter when the control system is time-invariant. Here, we briefly describe the structure of a port-Hamiltonian system.

A port-Hamiltonian system has the form:

$$\dot{\boldsymbol{x}} = [\mathcal{J}(\boldsymbol{x}) - \mathcal{R}(\boldsymbol{x})]\frac{\partial \mathcal{H}}{\partial \boldsymbol{x}} + \boldsymbol{g}(\boldsymbol{x})\boldsymbol{u} \tag{1}$$

$$\boldsymbol{y} = \boldsymbol{g}^{\mathrm{T}}(\boldsymbol{x})\frac{\partial \mathcal{H}}{\partial \boldsymbol{x}} \tag{2}$$

where $\boldsymbol{x}(t) \in \mathbb{R}^n$ is the state vector, $\mathcal{J}(\boldsymbol{x}) = -\mathcal{J}^{\mathrm{T}}(\boldsymbol{x})$ is an interconnection matrix which represents energy conserving interactions among the state variables, the matrix $\mathcal{R}(\boldsymbol{x}) = \mathcal{R}^{\mathrm{T}}(\boldsymbol{x}) \succeq 0$ accounts for the dissipation incurred during system motion, $\mathcal{H} : \mathbb{R}^n \to \mathbb{R}$ is the Hamiltonian function, and the matrix $\boldsymbol{g}(\boldsymbol{x}) \in \mathbb{R}^{n\times m}$ determines how the m inputs $\boldsymbol{u}(t) \in \mathbb{R}^m$ affect system motion. The vector $\boldsymbol{u}(t)$ of inputs and the vector $\boldsymbol{y}(t) \in \mathbb{R}^m$ of outputs are conjugate in the sense that their inner product expresses the power exchanged with external systems. The port-Hamiltonian system can be shown to be passive [7] by taking the Hamiltonian as a storage function:

$$\frac{\mathrm{d}\mathcal{H}(\boldsymbol{x})}{\mathrm{d}t} = \boldsymbol{y}^{\mathrm{T}}\boldsymbol{u} - \frac{\partial\mathcal{H}(\boldsymbol{x})}{\partial\boldsymbol{x}}^{\mathrm{T}}\mathcal{R}(\boldsymbol{x})\frac{\partial\mathcal{H}(\boldsymbol{x})}{\partial\boldsymbol{x}} \leq \boldsymbol{y}^{\mathrm{T}}\boldsymbol{u} \tag{3}$$

Given a PHS model, the control design objective is to construct a passive error system through feedback transformation.

3 Vehicle Motion Model

We consider a rigid aircraft with four inputs: the thrust force and three control moments in roll, pitch, and yaw. To define the equations of motion, we first establish two frames of reference. Let the orthonormal triad $\{\boldsymbol{i}_1, \boldsymbol{i}_2, \boldsymbol{i}_3\}$ define a reference frame whose axes point north, east, and downwards, respectively. Though this frame is Earth-fixed, we consider it "inertial enough" for the purpose of this work. Next, let the orthonormal triad $\{\boldsymbol{b}_1, \boldsymbol{b}_2, \boldsymbol{b}_3\}$ define a reference frame fixed at the center of mass of the aircraft with axes pointing through the nose, out the right wing, and through the belly of the vehicle, respectively. The orientation of the aircraft with respect to the inertial frame is given by the 3×3 proper rotation matrix $\mathbf{R}_{\mathrm{IB}}$ which transforms free vectors from the body frame to the inertial frame.

Let $\boldsymbol{v} = [u, v, w]^T$ represent the translational velocity of the aircraft with respect to inertial space, but expressed in the body frame, and let $\boldsymbol{p} = [p_1, p_2, p_3]^T = m\boldsymbol{v}$ denote the corresponding body translational momentum, where m is the aircraft mass. Let $\boldsymbol{\omega} = [p, q, r]^T$ represent the angular velocity of the aircraft with respect to inertial space, but expressed in the body frame, and let $\boldsymbol{h} = [h_1, h_2, h_3]^T = \boldsymbol{I}\boldsymbol{\omega}$ denote the corresponding body angular momentum, where the inertia matrix $\boldsymbol{I}$ takes the form

$$\boldsymbol{I} = \begin{bmatrix} I_{xx} & 0 & -I_{xz} \\ 0 & I_{yy} & 0 \\ -I_{xz} & 0 & I_{zz} \end{bmatrix}$$

It will sometimes be convenient to write

$$\begin{bmatrix} \boldsymbol{h} \\ \boldsymbol{p} \end{bmatrix} = \boldsymbol{\mathcal{M}} \begin{bmatrix} \boldsymbol{\omega} \\ \boldsymbol{v} \end{bmatrix} \qquad \text{where} \qquad \boldsymbol{\mathcal{M}} = \begin{bmatrix} \boldsymbol{I} & \mathbf{0}_{3\times3} \\ \mathbf{0}_{3\times3} & m\mathbb{I} \end{bmatrix} \tag{4}$$

where $\mathbb{I}$ is the 3×3 identity matrix.

Having earlier introduced the inertial and body reference frames, we now introduce a third – the wind frame – defined by the orthonormal triad $\{\boldsymbol{w}_1, \boldsymbol{w}_2, \boldsymbol{w}_3\}$. The wind frame is related to the body frame using the airspeed V, angle of attack α, and sideslip angle β, defined as follows

$$V = \|\boldsymbol{v}\|, \quad \beta = \arcsin\left(\frac{v}{V}\right), \quad \text{and} \quad \alpha = \arctan_4\left(\frac{w}{u}\right) \tag{5}$$

where $\arctan_4$ denotes the 4-quadrant arctangent. Note the definitions above define a transformation of the translational velocity variables $(u, v, w) \mapsto (V, \beta, \alpha)$ which is well-defined for $V > 0$ and $\beta \in (-\frac{\pi}{2}, \frac{\pi}{2})$. The proper rotation matrix mapping free vectors from the wind frame to the body frame is

$$\mathbf{R}_{\mathrm{BW}}(\alpha, \beta) = e^{-\hat{\boldsymbol{e}}_2\alpha}e^{\hat{\boldsymbol{e}}_3\beta} \tag{6}$$

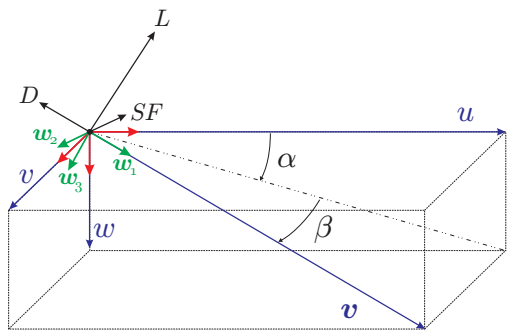

Figure 1: Aerodynamic angles for an aircraft

where $\boldsymbol{e}_i$ is the ith unit basis vector for $\mathbb{R}^3$ and the overhat indicates the 3×3 skew-symmetric "cross product equivalent matrix" which, for vectors $\boldsymbol{a}$ and $\boldsymbol{b}$, satisfies $\hat{\boldsymbol{a}}\boldsymbol{b} = \boldsymbol{a}\times\boldsymbol{b}$. Thus, for example,

$$\hat{\boldsymbol{e}}_2\alpha = \begin{bmatrix} 0 & 0 & \alpha \\ 0 & 0 & 0 \\ -\alpha & 0 & 0 \end{bmatrix} \quad \text{and} \quad e^{-\hat{\boldsymbol{e}}_2\alpha} = \begin{bmatrix} \cos\alpha & 0 & -\sin\alpha \\ 0 & 1 & 0 \\ \sin\alpha & 0 & \cos\alpha \end{bmatrix}$$

As with any rotation matrix, the inverse of the transformation is given by the transpose: $(e^{-\hat{\boldsymbol{e}}_2\alpha})^T = e^{-\hat{\boldsymbol{e}}_2^T\alpha} = e^{\hat{\boldsymbol{e}}_2\alpha}$.

The aircraft rotational and translational kinematic equations are

$$\dot{\mathbf{R}}_{\text{IB}} = \mathbf{R}_{\text{IB}}\hat{\boldsymbol{\omega}} \tag{7}$$

$$\dot{\boldsymbol{x}} = \mathbf{R}_{\text{IB}}\boldsymbol{v} \tag{8}$$

The former equation is typically expressed in terms of Euler angular rates corresponding to a common Euler angle parametrization for the rotation matrix $\mathbf{R}_{\text{IB}}$:

$$\mathbf{R}_{IB} = e^{\hat{\boldsymbol{e}}_3\psi}e^{\hat{\boldsymbol{e}}_2\theta}e^{\hat{\boldsymbol{e}}_1\phi} \tag{9}$$

Expressed in terms of the Euler angles, the rotational kinematic equations are well-defined provided $\theta \neq \pm\frac{\pi}{2}$.

Alternatively, as described by Battista *et al* [25], one may use the heading angle ψ together with the *tilt vector* $\boldsymbol{\zeta} = \mathbf{R}_{\text{IB}}^T\boldsymbol{i}_3$ to describe the attitude kinematics:

$$\begin{aligned} \dot{\boldsymbol{\zeta}} &= \boldsymbol{\zeta}\times\boldsymbol{\omega} \\ \dot{\psi} &= -\frac{1}{1-\zeta_1^2}\boldsymbol{\zeta}^T\hat{\boldsymbol{e}}_1\hat{\boldsymbol{e}}_1\boldsymbol{\omega} \end{aligned} \tag{10}$$

This alternative representation is well-defined provided $|\zeta_1| = |\boldsymbol{\zeta}^T\boldsymbol{e}_1| \neq 1$. That is, the parametrization is valid provided the body axis $\boldsymbol{b}_1$ is not aligned with the inertial vertical axis $\boldsymbol{i}_3$, precisely the same conditions under which the Euler angle parametrization holds.

For flight in still air, the dynamic equations expressed in the body-fixed reference frame are

$$\dot{\boldsymbol{h}} = \boldsymbol{h}\times\boldsymbol{\omega} + \boldsymbol{\tau}_{\text{c}} + \boldsymbol{\tau}_{\text{a}} \tag{11}$$

$$\dot{\boldsymbol{p}} = \boldsymbol{p}\times\boldsymbol{\omega} + mg\boldsymbol{\zeta} + \boldsymbol{f}_{\text{c}} + \boldsymbol{f}_{\text{a}} \tag{12}$$

where $\boldsymbol{f}_{\mathrm{a}}$ and $\boldsymbol{\tau}_{\mathrm{a}}$ represent the aerodynamic force and moment, respectively, while $\boldsymbol{f}_{\mathrm{c}}$ and $\boldsymbol{\tau}_{\mathrm{c}}$ represent the control force and moment. We assume the aircraft has a single thruster aligned with with its velocity such that $\boldsymbol{f}_{\mathrm{c}} = F_{\mathrm{c}}\,\boldsymbol{v}/V$, where F_{c} is the scalar thrust. The assumption that thrust is aligned with velocity is presumptuous, unless the propulsor is gimballed to enable vectored thrust. On the other hand, flight dynamic models typically assume thrust is aligned with the longitudinal axis, even when the assumption is inaccurate. In any case, one should verify that a control law relying on such an assumption is effective even when the assumption is relaxed.

We assume the aerodynamic force and moment are governed by quasi-steady flow, depending only on the translational and rotational velocity. Rather than adopt explicit analytical expressions for aerodynamic effects, however, we make only generic assumptions. For example, we assume the aerodynamic moment opposes rotation and vanishes when the motion is purely translational: $\boldsymbol{\tau}_{\mathrm{a}} \cdot \boldsymbol{\omega} < 0$ when $\boldsymbol{\omega} \neq \mathbf{0}$ and $\boldsymbol{\tau}_{\mathrm{a}} = \mathbf{0}$ when $\boldsymbol{\omega} = \mathbf{0}$. In reality, there are important aerodynamic moments that arise solely from translational motion, such as the "weathervane" moments in pitch and yaw. Rather than account for these bare airframe effects early in the modeling process, we absorb them into the three-axis control moment to be defined shortly. To implement the resulting control law, one must first remove these moment contributions due to the aerodynamics of the bare airframe.

The aerodynamic force is typically expressed in wind frame components: the drag force, which opposes velocity; the lift force, which acts normal to drag and in the aircraft plane of symmetry; and the side force, which is normal to the two other components. These components are assumed to depend solely on the aerodynamic angles. In reality, small aerodynamic forces also arise in response to aircraft rotation. For example, an aircraft rotating in yaw will experience a small side force due to the vertical stabilizer; this small force, acting about the center of gravity through a large moment arm, provides a yaw damping moment. We ignore these small aerodynamic forces due to rotational motion, although we retain the aerodynamic moments that they generate, in the control design and analysis; the small aerodynamic forces are included in simulations.

For a given (constant) air density ρ and wing planform area S, the aerodynamic force expressed in the body reference frame can be written as:

$$\boldsymbol{f}_{\mathrm{a}}(\boldsymbol{v}) = -\frac{1}{2}\rho S V^2 \mathbf{R}_{\mathrm{BW}}(\alpha,\beta)\boldsymbol{C}(\alpha,\beta) \tag{13}$$

where $\boldsymbol{C}(\alpha,\beta) = [C_{\mathrm{D}}(\alpha,\beta), C_S(\alpha,\beta), C_L(\alpha,\beta)]^T$ contains the indicated nondimensional aerodynamic force coefficients. These are assumed to exhibit the following properties:

- The drag coefficient, $C_{\mathrm{D}}(\alpha,\beta)$, is a positive function and even in both arguments.
- The side force coefficient, $C_S(\alpha,\beta)$, is a smooth, odd function with respect to β. It is positive (respectively, negative) when when $e^{i\beta}$ lies in the first (respectively, fourth) quadrant of the complex plane [1].
- The lift coefficient, $C_L(\alpha,\beta)$, is a smooth function and nondecreasing with respect to α.

While the third condition given above allows a diminishing slope of the lift coefficient near the stall angle of attack, it prohibits the decrease in lift coefficient that occurs with increasing angle of attack beyond the stall condition. Thus, while the aerodynamic model is quite general in its representation of normal flight conditions, the subsequent analysis and results require (and help to ensure) that the aircraft operates below the stall condition.

[1] Note that the sign of C_S is opposite the standard convention for lateral force coefficient.

Using the definitions of aerodynamic angles in equations (5) and (6), we can reformulate the aerodynamic forces:

$$\boldsymbol{f}_{\mathrm{a}}(\boldsymbol{v}) = -\varrho \begin{bmatrix} uVC_D - \frac{uvV}{\sqrt{u^2+w^2}}C_S - \frac{wV^2}{\sqrt{u^2+w^2}}C_L \\ vVC_D + V\sqrt{u^2+w^2}C_S \\ wVC_D - \frac{vwV}{\sqrt{u^2+w^2}}C_S + \frac{uV^2}{\sqrt{u^2+w^2}}C_L \end{bmatrix} \tag{14}$$

where $\varrho = \frac{1}{2}\rho S$ is assumed to be constant and the drag, side-force and lift coefficients depend on the velocity $\boldsymbol{v}$. Equation (14) can be further decomposed as follows:

$$\boldsymbol{f}_{\mathrm{a}}(\boldsymbol{v}) = \left(\hat{\boldsymbol{J}}_v - \mathcal{R}_v\right)\boldsymbol{v} \tag{15}$$

where $\boldsymbol{J}_v = \frac{\varrho V}{\sqrt{u^2+w^2}}\left[wC_S, VC_L, -uC_S\right]^{\mathrm{T}}$ accounts for a force orthogonal to the velocity vector (i.e., a turning force) and where the matrix $\mathcal{R}_v = \varrho V C_D \mathbb{I}_{3\times 3} \succ 0$ relates to the dissipation of translational kinetic energy.

Let $\boldsymbol{\eta} = \left[\boldsymbol{\zeta}^{\mathrm{T}}, \psi, \boldsymbol{q}^{\mathrm{T}}\right]^{\mathrm{T}}$ be the configuration vector, where $\boldsymbol{q}$ denotes the position of the aircraft in inertial space, and let $\boldsymbol{\nu} = \left[\boldsymbol{h}^{\mathrm{T}}, \boldsymbol{p}^{\mathrm{T}}\right]^{\mathrm{T}}$ be the generalized momentum vector. We concatenate configuration and momentum into the state vector $\boldsymbol{x} = \left[\boldsymbol{\nu}^{\mathrm{T}}, \boldsymbol{\eta}^{\mathrm{T}}\right]^{\mathrm{T}}$.

Proposition 1. The system dynamics (8), (10), (11), and (12) can be written in the PHS form (1-2) with Hamiltonian

$$\mathcal{H} = \frac{1}{2}\boldsymbol{\nu}^{\mathrm{T}}\mathcal{M}^{-1}\boldsymbol{\nu} - mg\boldsymbol{e}_3^{\mathrm{T}}\boldsymbol{q} \tag{16}$$

and with

$$\mathcal{J} = \begin{bmatrix} \hat{\boldsymbol{h}} & \hat{\boldsymbol{p}} & \hat{\boldsymbol{\zeta}} & -\boldsymbol{a}(\boldsymbol{\zeta})^{\mathrm{T}} & \boldsymbol{0} \\ \hat{\boldsymbol{p}} & \hat{\boldsymbol{J}}_v & \boldsymbol{0} & \boldsymbol{0} & -\mathbf{R}_{IB}^{\mathrm{T}} \\ \hat{\boldsymbol{\zeta}} & \boldsymbol{0} & \boldsymbol{0} & \boldsymbol{0} & \boldsymbol{0} \\ \boldsymbol{a}(\boldsymbol{\zeta}) & \boldsymbol{0} & \boldsymbol{0} & 0 & \boldsymbol{0} \\ \boldsymbol{0} & \mathbf{R}_{IB} & \boldsymbol{0} & \boldsymbol{0} & \boldsymbol{0} \end{bmatrix} \tag{17}$$

$$\mathcal{R} = \begin{bmatrix} \boldsymbol{D}_\omega & \boldsymbol{0} & \boldsymbol{0} & \boldsymbol{0} & \boldsymbol{0} \\ \boldsymbol{0} & \mathcal{R}_v & \boldsymbol{0} & \boldsymbol{0} & \boldsymbol{0} \\ \boldsymbol{0} & \boldsymbol{0} & \boldsymbol{0} & \boldsymbol{0} & \boldsymbol{0} \\ \boldsymbol{0} & \boldsymbol{0} & \boldsymbol{0} & 0 & \boldsymbol{0} \\ \boldsymbol{0} & \boldsymbol{0} & \boldsymbol{0} & \boldsymbol{0} & \boldsymbol{0} \end{bmatrix} \tag{18}$$

$$\boldsymbol{g} = \begin{bmatrix} \mathbb{I} & \boldsymbol{0} & \boldsymbol{0} & \boldsymbol{0} & \boldsymbol{0} \\ \boldsymbol{0} & \frac{\boldsymbol{v}^{\mathrm{T}}}{V} & \boldsymbol{0} & 0 & \boldsymbol{0} \end{bmatrix}^{\mathrm{T}} \tag{19}$$

Here $\mathbf{R}_{IB}$ depends on both $\boldsymbol{\zeta}$ and ψ and $\boldsymbol{a}(\boldsymbol{\zeta})$ is derived from equation (10):

$$\boldsymbol{a}(\boldsymbol{\zeta}) = -\frac{1}{1-\zeta_1^2}\boldsymbol{\zeta}^{\mathrm{T}}\hat{\boldsymbol{e}}_1\hat{\boldsymbol{e}}_1 \tag{20}$$

Note that this PHS formulation holds for aerodynamic coefficients C_D, C_S, and C_L of any functional form.

4 Directional Stabilization

The procedure followed in this paper is inspired by the work of Fujimoto *et al* [24], whose paper describes a trajectory tracking control strategy for port-Hamiltonian systems in which a passive error dynamic system is constructed via canonical transformation.

The goal in this section is to stabilize the aircraft's motion to non-slipping, wings-level flight in a specified direction described by a desired course angle χ_{d} and a desired climb angle γ_{d} (with $\gamma_{\mathrm{d}} \neq \pm\frac{\pi}{2}$). Thus, we seek to attain the following conditions:

$$\beta = 0,\ \phi = 0,\ \theta = \alpha_d + \gamma_{\mathrm{d}},\ \psi = \chi_{\mathrm{d}}$$

Rather than specify the desired airspeed and solve for the desired angle of attack, we specify the desired angle of attack α_{d} instead and then solve for the corresponding airspeed V_{d}. The former approach would require knowledge of the explicit functional forms for the aerodynamic coefficients to solve for the angle of attack. In addition, specifying the angle of attack allows one to avoid inadvertently exceeding the stall condition by, for example, specifying an airspeed and climb angle for which the corresponding angle of attack exceeds the critical value for stall. Recall that the model for the lift coefficient C_L only captures the pre-stall decrease in slope. Stall is avoided through the judicious choice of the nominal flight condition and prescribed bounds on the initial state; see the discussion of stability analysis following Theorem 1.

The desired velocity vector is $\boldsymbol{v}_{\mathrm{d}} = V_{\mathrm{d}}(\cos\alpha_{\mathrm{d}}, 0, \sin\alpha_{\mathrm{d}})^{\mathrm{T}}$. Given a desired climb angle, selecting α_{d} also fixes the desired pitch angle, or equivalently the desired tilt vector since the desired roll angle is zero:

$$\boldsymbol{\zeta}_{\mathrm{d}} = [-\sin(\alpha_{\mathrm{d}} + \gamma_{\mathrm{d}}),\ 0,\ \cos(\alpha_{\mathrm{d}} + \gamma_{\mathrm{d}})]^T \tag{21}$$

The angular velocity is zero in the desired state of steady, wings level flight at a fixed attitude. As for the translational velocity, the airspeed is chosen in such a way that the aerodynamic forces balance the component of gravitational force along the $\boldsymbol{b}_3$ axis:

$$\boldsymbol{v}_{\mathrm{d}} = \sqrt{\frac{mg\cos\gamma_{\mathrm{d}}}{\varrho C_{L_{\mathrm{d}}}}}(\cos\alpha_{\mathrm{d}}, 0, \sin\alpha_{\mathrm{d}})^{\mathrm{T}} \tag{22}$$

where $C_{L_{\mathrm{d}}}$ is the lift coefficient evaluated at steady state.

While (22) represents the desired velocity when the attitude is at steady state, using it as the immediate control objective may yield poor performance, and violate conditions required in the proof of stability. Instead, target values denoted with the subscript "t" are designed which converge to the desired values at steady state.

Define the function:

$$\begin{aligned}\mathcal{H}_{\mathrm{c}} =& \frac{1}{2}(\boldsymbol{h} - \boldsymbol{I}\boldsymbol{\omega}_{\mathrm{t}})^{\mathrm{T}}\boldsymbol{I}^{-1}(\boldsymbol{h} - \boldsymbol{I}\boldsymbol{\omega}_{\mathrm{t}}) + \frac{m}{2}(V - V_{\mathrm{t}})^2 + \mathcal{V}_{\mathrm{d}} \\ &+ \frac{mV_{\mathrm{d}}^2}{2}\left((\sin\alpha - \sin\alpha_{\mathrm{d}})^2 + 2(1 - \cos\beta)\right)\end{aligned} \tag{23}$$

where $\mathcal{V}_{\mathrm{d}} = \frac{1}{2}(k_\zeta(\boldsymbol{\zeta} - \boldsymbol{\zeta}_{\mathrm{d}})^{\mathrm{T}}(\boldsymbol{\zeta} - \boldsymbol{\zeta}_{\mathrm{d}}) + k_\psi(\psi - \psi_{\mathrm{d}})^2)$ is an artificial potential with $k_\zeta, k_\psi > 0$ and where

$$\boldsymbol{\omega}_{\mathrm{t}} = \left[-\frac{g\zeta_2\cos\beta}{V_{\mathrm{t}}\sin\alpha_{\mathrm{d}}},\ 0,\ 0\right]^T, \tag{24}$$

and

$$\begin{aligned}&V_{\mathrm{t}}(\alpha, \beta, \boldsymbol{\zeta}) = \\ &\sqrt{\frac{mg}{\varrho C_{L_{\mathrm{d}}}}\left(\boldsymbol{e}_3^{\mathrm{T}}\mathbf{R}_{\mathrm{BW}}^{\mathrm{T}}\boldsymbol{\zeta} + \frac{\sin\beta}{\sin\alpha_{\mathrm{d}}}\left(\cos\alpha - \frac{\cos\beta}{\cos\alpha}\right)\zeta_2\cos\beta\right)}\end{aligned} \tag{25}$$

Note that $\mathcal{H}_\mathrm{c}$ can be split into $\mathcal{H}_h$, which contains information about the tracking error of the angular dynamics, $\mathcal{H}_p$, which contains information about the tracking error of the translational dynamics and $\mathcal{V}_\mathrm{d}$, which quantifies the error in the pitch and heading:

$$\begin{aligned}
\mathcal{H}_h =& \frac{1}{2}(\boldsymbol{h} - \boldsymbol{I}\boldsymbol{\omega}_\mathrm{t})^\mathrm{T}\boldsymbol{I}^{-1}(\boldsymbol{h} - \boldsymbol{I}\boldsymbol{\omega}_\mathrm{t}) && (26)\\
\mathcal{H}_p =& \frac{m}{2}\left((V - V_\mathrm{t})^2\right.\\
&\left.+V_\mathrm{d}^2\left((\sin\alpha - \sin\alpha_\mathrm{d})^2 + 2(1-\cos\beta)\right)\right) && (27)\\
\mathcal{V}_\mathrm{d} =& \frac{1}{2}(k_\zeta(\boldsymbol{\zeta} - \boldsymbol{\zeta}_\mathrm{d})^\mathrm{T}(\boldsymbol{\zeta} - \boldsymbol{\zeta}_\mathrm{d}) + k_\psi(\psi - \psi_\mathrm{d})^2) && (28)
\end{aligned}$$

Here and below, the velocity components V, α, and β should be interpreted as functions of the translational momentum p.

Theorem 1. Consider the control law

$$\begin{aligned}
\boldsymbol{\tau}_\mathrm{c} =& -\begin{bmatrix}\mathbb{I} & -\boldsymbol{I}\frac{\partial\boldsymbol{\omega}_\mathrm{t}}{\partial\boldsymbol{p}} & -\boldsymbol{I}\frac{\partial\boldsymbol{\omega}_\mathrm{t}}{\partial\boldsymbol{\eta}}\end{bmatrix}(\mathcal{J}-\mathcal{R})\frac{\partial\tilde{\mathcal{H}}}{\partial\boldsymbol{x}}^\mathrm{T}\\
&-\boldsymbol{I}\frac{\partial\boldsymbol{\omega}_\mathrm{t}}{\partial\boldsymbol{x}}(\mathcal{J}-\mathcal{R})^\mathrm{T}\begin{bmatrix}\boldsymbol{0} & \frac{\partial\mathcal{H}_p}{\partial\mathbf{p}} & \frac{\partial(\mathcal{V}_\mathrm{d}+\mathcal{H})}{\partial\boldsymbol{x}}\end{bmatrix}^\mathrm{T}\\
&-\mathcal{C}(\boldsymbol{\omega} - \boldsymbol{\omega}_\mathrm{t}) && (29)
\end{aligned}$$

and

$$\begin{aligned}
F_\mathrm{c} =& \varrho C_D V_\mathrm{t}^2 - mg\frac{\boldsymbol{v}^\mathrm{T}\boldsymbol{\zeta}}{V} + m\begin{bmatrix}\boldsymbol{0} & \frac{\partial V_\mathrm{t}}{\partial\boldsymbol{p}} & \frac{\partial V_\mathrm{t}}{\partial\boldsymbol{\eta}}\end{bmatrix}(\mathcal{J}-\mathcal{R})\frac{\partial\tilde{\mathcal{H}}}{\partial\boldsymbol{x}}^\mathrm{T}\\
&+V_\mathrm{d}^2\left(\frac{\cos\alpha(\sin\alpha - \sin\alpha_\mathrm{d})}{\cos\beta}\left(\frac{mg}{VV_\mathrm{t}}\boldsymbol{e}_3^\mathrm{T}\boldsymbol{R}_\mathrm{BW}^\mathrm{T}\boldsymbol{\zeta} - \varrho C_{L_\mathrm{d}}\right)\right.\\
&\left.+\frac{mg\sin\beta}{VV_\mathrm{t}}\zeta_2\cos\beta\right) && (30)
\end{aligned}$$

where $\tilde{\mathcal{H}} = \mathcal{H} - \mathcal{H}_\mathrm{c}$ and $\mathcal{C} \succ 0$. The control law asymptotically stabilizes the desired equilibrium.

Remark 1. Implementing the control law requires knowledge of the aerodynamic model, but the proof does not rely on an explicit functional form for the aerodynamic forces and moments. See the comments following (13).

Proof. Taking $\mathcal{H}_\mathrm{c}$ as a candidate Lyapunov function,

$$\begin{aligned}
\dot{\mathcal{H}}_\mathrm{c} &= \frac{\partial\mathcal{H}_\mathrm{c}}{\partial\boldsymbol{x}}\left((\mathcal{J}-\mathcal{R})\frac{\partial\mathcal{H}}{\partial\boldsymbol{x}}^\mathrm{T} + \boldsymbol{g}\boldsymbol{u}\right)\\
&= \frac{\partial\mathcal{H}_\mathrm{c}}{\partial\boldsymbol{x}}\left((\mathcal{J}-\mathcal{R})\frac{\partial\tilde{\mathcal{H}}}{\partial\boldsymbol{x}}^\mathrm{T} + \boldsymbol{g}\boldsymbol{u}\right) - \frac{\partial\mathcal{H}_\mathrm{c}}{\partial\boldsymbol{x}}\mathcal{R}\frac{\partial\mathcal{H}_\mathrm{c}}{\partial\boldsymbol{x}}^\mathrm{T}\\
&\leq \frac{\partial\mathcal{H}_\mathrm{c}}{\partial\boldsymbol{x}}\left((\mathcal{J}-\mathcal{R})\frac{\partial\tilde{\mathcal{H}}}{\partial\boldsymbol{x}}^\mathrm{T} + \boldsymbol{g}\boldsymbol{u}\right) && (31)
\end{aligned}$$

With the proposed control moment, $\boldsymbol{\tau}_\mathrm{c}$, in equation (29), the time derivative of the proposed Hamiltonian

function becomes:

$$\dot{\mathcal{H}}_{\mathrm{c}} = -\frac{\partial \mathcal{H}_{\mathrm{c}}}{\partial \boldsymbol{x}} \mathcal{R} \frac{\partial \mathcal{H}_{\mathrm{c}}}{\partial \boldsymbol{x}}^{\mathrm{T}} - (\boldsymbol{\omega} - \boldsymbol{\omega}_{\mathrm{t}})^{\mathrm{T}} \mathcal{C} (\boldsymbol{\omega} - \boldsymbol{\omega}_{\mathrm{t}}) + \begin{bmatrix} \mathbf{0} \\ \frac{\partial \mathcal{H}_p}{\partial \boldsymbol{p}}^{\mathrm{T}} \\ \frac{\partial \mathcal{V}_{\mathrm{d}}}{\partial \boldsymbol{\eta}}^{\mathrm{T}} + \frac{\partial \mathcal{H}_p}{\partial \boldsymbol{\eta}}^{\mathrm{T}} \end{bmatrix}^{\mathrm{T}} (\mathcal{J} - \mathcal{R}) \begin{bmatrix} \boldsymbol{\omega}_{\mathrm{t}} \\ \boldsymbol{v} - \frac{\partial \mathcal{H}_p}{\partial \boldsymbol{p}}^{\mathrm{T}} \\ \frac{\partial \mathcal{V}}{\partial \boldsymbol{\eta}}^{\mathrm{T}} - \frac{\partial \mathcal{V}_{\mathrm{d}}}{\partial \boldsymbol{\eta}}^{\mathrm{T}} - \frac{\partial \mathcal{H}_p}{\partial \boldsymbol{\eta}}^{\mathrm{T}} \end{bmatrix} \tag{32}$$

Adding and subtracting the term $\frac{\partial \mathcal{H}_p}{\partial \boldsymbol{x}} (\mathcal{J} - \mathcal{R}) \frac{\partial \mathcal{H}_p}{\partial \boldsymbol{x}}^{\mathrm{T}}$ and making use of the following relations:

$$\frac{\partial \mathcal{V}_{\mathrm{d}}}{\partial \boldsymbol{x}} \mathcal{R} \frac{\partial \mathcal{V}_{\mathrm{d}}}{\partial \boldsymbol{x}}^{\mathrm{T}} = 0, \qquad \frac{\partial \mathcal{H}_p}{\partial \boldsymbol{x}} \mathcal{J} \frac{\partial \mathcal{H}_p}{\partial \boldsymbol{x}}^{\mathrm{T}} = 0$$

$$\begin{bmatrix} \mathbf{0} \\ \frac{\partial \mathcal{H}_p}{\partial \boldsymbol{p}}^{\mathrm{T}} \\ \frac{\partial \mathcal{V}_{\mathrm{d}}}{\partial \boldsymbol{\eta}}^{\mathrm{T}} + \frac{\partial \mathcal{H}_p}{\partial \boldsymbol{\eta}}^{\mathrm{T}} \end{bmatrix}^{\mathrm{T}} (\mathcal{J} - \mathcal{R}) \begin{bmatrix} \mathbf{0} \\ \mathbf{0} \\ -\frac{\partial \mathcal{V}_{\mathrm{d}}}{\partial \boldsymbol{\eta}}^{\mathrm{T}} - \frac{\partial \mathcal{H}_p}{\partial \boldsymbol{\eta}}^{\mathrm{T}} \end{bmatrix} = 0$$

reduces equation (32) to

$$\dot{\mathcal{H}}_{\mathrm{c}} = -\frac{\partial \mathcal{H}_h}{\partial \boldsymbol{x}} \mathcal{R} \frac{\partial \mathcal{H}_h}{\partial \boldsymbol{x}}^{\mathrm{T}} - (\boldsymbol{\omega} - \boldsymbol{\omega}_{\mathrm{t}})^{\mathrm{T}} \mathcal{C} (\boldsymbol{\omega} - \boldsymbol{\omega}_{\mathrm{t}}) + \begin{bmatrix} \mathbf{0} \\ \frac{\partial \mathcal{H}_p}{\partial \boldsymbol{p}}^{\mathrm{T}} \\ \frac{\partial \mathcal{V}_{\mathrm{d}}}{\partial \boldsymbol{\eta}}^{\mathrm{T}} + \frac{\partial \mathcal{H}_p}{\partial \boldsymbol{\eta}}^{\mathrm{T}} \end{bmatrix}^{\mathrm{T}} (\mathcal{J} - \mathcal{R}) \begin{bmatrix} \boldsymbol{\omega}_{\mathrm{t}} \\ \boldsymbol{v} \\ \frac{\partial \mathcal{V}}{\partial \boldsymbol{\eta}}^{\mathrm{T}} \end{bmatrix} \tag{33}$$

Expanding (33) gives:

$$\begin{aligned} \dot{\mathcal{H}}_{\mathrm{c}} = & -\frac{\partial \mathcal{H}_h}{\partial \boldsymbol{x}} \mathcal{R} \frac{\partial \mathcal{H}_h}{\partial \boldsymbol{x}}^{\mathrm{T}} - (\boldsymbol{\omega} - \boldsymbol{\omega}_{\mathrm{t}})^{\mathrm{T}} \mathcal{C} (\boldsymbol{\omega} - \boldsymbol{\omega}_{\mathrm{t}}) \\ & + (V - V_{\mathrm{t}}) \left(-\varrho V^2 C_D + \frac{mg}{V} \boldsymbol{v}^{\mathrm{T}} \boldsymbol{\zeta} + F_{\mathrm{c}} \right) \\ & + \left(V_{\mathrm{d}}^2 \sin\beta - (V - V_{\mathrm{t}}) \frac{\partial V_{\mathrm{t}}}{\partial \beta} \right) \\ & \quad \left(\frac{mg}{V} \boldsymbol{e}_2^{\mathrm{T}} \boldsymbol{R}_{\mathrm{BW}} \boldsymbol{\zeta} - \varrho V C_S - m \boldsymbol{e}_3^{\mathrm{T}} \boldsymbol{R}_{\mathrm{BW}} \boldsymbol{\omega}_{\mathrm{t}} \right) \\ & + \left(\frac{V_{\mathrm{d}}^2 (\sin\alpha - \sin\alpha_{\mathrm{d}}) \cos\alpha}{\cos\beta} - (V - V_{\mathrm{t}}) \frac{\partial V_{\mathrm{t}}}{\partial \alpha} \right) \\ & \quad \left(-\varrho V C_L + m \boldsymbol{e}_2^{\mathrm{T}} \boldsymbol{R}_{\mathrm{BW}} \boldsymbol{\omega}_{\mathrm{t}} + \frac{mg}{V} \boldsymbol{e}_3^{\mathrm{T}} \boldsymbol{R}_{\mathrm{BW}} \boldsymbol{\zeta} \right) \\ & + \left(k_{\zeta} (\boldsymbol{\zeta} - \boldsymbol{\zeta}_{\mathrm{d}})^{\mathrm{T}} - m (V - V_{\mathrm{t}}) \frac{\partial V_{\mathrm{t}}}{\partial \boldsymbol{\zeta}} \right) \hat{\boldsymbol{\zeta}} \boldsymbol{\omega}_{\mathrm{t}} \\ & + k_{\psi} (\psi - \psi_{\mathrm{d}}) \boldsymbol{a}(\boldsymbol{\zeta}) \boldsymbol{\omega}_{\mathrm{t}} \end{aligned} \tag{34}$$

Substituting for the control thrust F_{c} from equation (30), equation (34) becomes:

$$\begin{aligned}\dot{\mathcal{H}}_{\mathrm{c}} = &- \frac{\partial \mathcal{H}_h}{\partial \boldsymbol{x}} \mathcal{R} \frac{\partial \mathcal{H}_h}{\partial \boldsymbol{x}}^{\mathrm{T}} - (\boldsymbol{\omega} - \boldsymbol{\omega}_{\mathrm{t}})^{\mathrm{T}} \mathcal{C} (\boldsymbol{\omega} - \boldsymbol{\omega}_{\mathrm{t}}) \\ &- \varrho C_D (V - V_{\mathrm{t}})(V^2 - V_{\mathrm{t}}^2) \\ &+ V_{\mathrm{d}}^2 \sin\beta \left(\frac{mg\zeta_2 \cos\beta}{V_{\mathrm{t}}} - \varrho V C_S - m \boldsymbol{e}_3^{\mathrm{T}} \boldsymbol{R}_{\mathrm{BW}} \boldsymbol{\omega}_{\mathrm{t}} \right. \\ &\quad \left. - \frac{mg \sin\beta (\zeta_1 \cos\alpha + \zeta_3 \sin\alpha)}{V} \right) \\ &+ \frac{V_{\mathrm{d}}^2 (\sin\alpha - \sin\alpha_{\mathrm{d}}) \cos\alpha}{\cos\beta} \\ &\quad \left(-\varrho V_{\mathrm{t}} C_L + m \boldsymbol{e}_2^{\mathrm{T}} \boldsymbol{R}_{\mathrm{BW}} \boldsymbol{\omega}_{\mathrm{t}} + \frac{mg}{V_{\mathrm{t}}} \boldsymbol{e}_3^{\mathrm{T}} \boldsymbol{R}_{\mathrm{BW}} \boldsymbol{\zeta} \right) \\ &+ k_\zeta (\boldsymbol{\zeta} - \boldsymbol{\zeta}_{\mathrm{d}})^{\mathrm{T}} \hat{\boldsymbol{\zeta}} \boldsymbol{\omega}_{\mathrm{t}} + k_\psi (\psi - \psi_{\mathrm{d}}) \boldsymbol{a}(\boldsymbol{\zeta}) \boldsymbol{\omega}_{\mathrm{t}} \end{aligned} \tag{35}$$

Taking $\omega_{2_{\mathrm{t}}} = \omega_{3_{\mathrm{t}}} = 0$ eliminates the last term of (35) and reduces it to

$$\begin{aligned}\dot{\mathcal{H}}_{\mathrm{c}} = &- \frac{\partial \mathcal{H}_h}{\partial \boldsymbol{x}} \mathcal{R} \frac{\partial \mathcal{H}_h}{\partial \boldsymbol{x}}^{\mathrm{T}} - (\boldsymbol{\omega} - \boldsymbol{\omega}_{\mathrm{t}})^{\mathrm{T}} \mathcal{C} (\boldsymbol{\omega} - \boldsymbol{\omega}_{\mathrm{t}}) \\ &- \varrho C_D (V - V_{\mathrm{t}})^2 (V + V_{\mathrm{t}}) + \zeta_2 \zeta_{3_{\mathrm{d}}} \omega_{1_{\mathrm{t}}} \\ &+ V_{\mathrm{d}}^2 \sin\beta \left(m \boldsymbol{\omega}_{1_{\mathrm{t}}} \sin\alpha - \varrho V C_S + \frac{mg\zeta_2 \cos\beta}{V_{\mathrm{t}}} \right. \\ &\quad \left. - \frac{mg \sin\beta (\zeta_1 \cos\alpha + \zeta_3 \sin\alpha)}{V} \right) \\ &+ \frac{V_{\mathrm{d}}^2 (\sin\alpha - \sin\alpha_{\mathrm{d}}) \cos\alpha}{\cos\beta} \\ &\quad \left(-\varrho V_{\mathrm{t}} C_L - m \boldsymbol{\omega}_{1_{\mathrm{t}}} \cos\alpha \sin\beta + \frac{mg}{V_{\mathrm{t}}} \boldsymbol{e}_3^{\mathrm{T}} \boldsymbol{R}_{\mathrm{BW}} \boldsymbol{\zeta} \right) \end{aligned} \tag{36}$$

One may use $\omega_{1_{\mathrm{t}}}$ to eliminate undesired terms involving $V_{\mathrm{d}} \sin\beta$. However, $\omega_{1_{\mathrm{t}}}$ is multiplied by $\sin\alpha$ whose value can pass through zero during transient motion. To resolve this issue, take the term $V_{\mathrm{d}}^2 \sin\beta (\sin\alpha - \sin\alpha_{\mathrm{d}}) m \boldsymbol{\omega}_{1_{\mathrm{t}}}$ away from the third line of (36) and add it to the last line:

$$\begin{aligned}\dot{\mathcal{H}}_{\mathrm{c}} = &- \frac{\partial \mathcal{H}_h}{\partial \boldsymbol{x}} \mathcal{R} \frac{\partial \mathcal{H}_h}{\partial \boldsymbol{x}}^{\mathrm{T}} - (\boldsymbol{\omega} - \boldsymbol{\omega}_{\mathrm{t}})^{\mathrm{T}} \mathcal{C} (\boldsymbol{\omega} - \boldsymbol{\omega}_{\mathrm{t}}) \\ &- \varrho C_D (V - V_{\mathrm{t}})^2 (V + V_{\mathrm{t}}) + \zeta_2 \zeta_{3_{\mathrm{d}}} \omega_{1_{\mathrm{t}}} \\ &+ V_{\mathrm{d}}^2 \sin\beta \left(m \boldsymbol{\omega}_{1_{\mathrm{t}}} \sin\alpha_{\mathrm{d}} - \varrho V C_S + \frac{mg\zeta_2 \cos\beta}{V_{\mathrm{t}}} \right. \\ &\quad \left. - \frac{mg \sin\beta (\zeta_1 \cos\alpha + \zeta_3 \sin\alpha)}{V} \right) \\ &+ \frac{V_{\mathrm{d}}^2 (\sin\alpha - \sin\alpha_{\mathrm{d}}) \cos\alpha}{\cos\beta} \left(\frac{mg}{V_{\mathrm{t}}} \boldsymbol{e}_3^{\mathrm{T}} \boldsymbol{R}_{\mathrm{BW}} \boldsymbol{\zeta} \right. \\ &\quad \left. - \varrho V_{\mathrm{t}} C_L - m \boldsymbol{\omega}_{1_{\mathrm{t}}} \sin\beta \left(\cos\alpha - \frac{\cos\beta}{\cos\alpha} \right) \right) \end{aligned} \tag{37}$$

Substituting (24) in (37) gives:

$$\begin{aligned}\dot{\mathcal{H}}_{\mathrm{c}} = &- \frac{\partial \mathcal{H}_h}{\partial \boldsymbol{x}} \mathcal{R} \frac{\partial \mathcal{H}_h}{\partial \boldsymbol{x}}^{\mathrm{T}} - (\boldsymbol{\omega} - \boldsymbol{\omega}_{\mathrm{t}})^{\mathrm{T}} \mathcal{C} (\boldsymbol{\omega} - \boldsymbol{\omega}_{\mathrm{t}}) \\ &- \varrho C_D (V - V_{\mathrm{t}})^2 (V + V_{\mathrm{t}}) - \frac{mg\zeta_2^2 \zeta_{3_{\mathrm{d}}} \cos\beta}{V_{\mathrm{t}} \sin\alpha_{\mathrm{d}}} \\ &- V_{\mathrm{d}}^2 \sin\beta \left(\varrho V C_{SF} + \frac{g \sin\beta}{V} (\zeta_1 \cos\alpha + \zeta_3 \sin\alpha) \right) \\ &+ \frac{V_{\mathrm{d}}^2 (\sin\alpha - \sin\alpha_{\mathrm{d}}) \cos\alpha}{\cos\beta} \Bigg(- \varrho V_{\mathrm{t}} C_L \\ &+ \frac{mg}{V_{\mathrm{t}}} \left(\boldsymbol{e}_3^{\mathrm{T}} \boldsymbol{R}_{\mathrm{BW}} \boldsymbol{\zeta} + \frac{\zeta_2 \cos\beta \sin\beta}{\sin\alpha_{\mathrm{d}}} \left(\cos\alpha - \frac{\cos\beta}{\cos\alpha} \right) \right) \Bigg)\end{aligned} \tag{38}$$

Finally, substituting (25) in the bottom line of (38) gives:

$$\begin{aligned}\dot{\mathcal{H}}_{\mathrm{c}} = &- \frac{\partial \mathcal{H}_h}{\partial \boldsymbol{x}} \mathcal{R} \frac{\partial \mathcal{H}_h}{\partial \boldsymbol{x}}^{\mathrm{T}} - (\boldsymbol{\omega} - \boldsymbol{\omega}_{\mathrm{t}})^{\mathrm{T}} \mathcal{C} (\boldsymbol{\omega} - \boldsymbol{\omega}_{\mathrm{t}}) \\ &- \varrho C_D (V - V_{\mathrm{t}})^2 (V + V_{\mathrm{t}}) - \frac{g\zeta_2^2 \zeta_{3_{\mathrm{d}}} \cos\beta}{V_{\mathrm{t}} \sin\alpha_{\mathrm{d}}} \\ &- \frac{V_{\mathrm{d}}^2 \sin\beta}{V} \left(\varrho V^2 C_{SF} + mg \sin\beta (\zeta_1 \cos\alpha + \zeta_3 \sin\alpha) \right) \\ &- \frac{\varrho V_{\mathrm{t}} V_{\mathrm{d}}^2 (\sin\alpha - \sin\alpha_{\mathrm{d}}) \left(C_L - C_{L_{\mathrm{d}}} \right) \cos\alpha}{\cos\beta}\end{aligned} \tag{39}$$

Note that the first two terms are non-positive since $\mathcal{R} \succeq 0$ and $\mathcal{C} \succ 0$. In addition, the facts that C_D is positive and that V and V_{t} are non-negative mean that $-\varrho C_D (V - V_{\mathrm{t}})^2 (V + V_{\mathrm{t}}) \leq 0$. Moreover, the term $-\frac{g\zeta_2^2 \zeta_{3_{\mathrm{d}}} \cos\beta}{V_{\mathrm{t}} \sin\alpha_{\mathrm{d}}}$ is also nonpositive since all the terms besides ζ_2 are greater than zero. Furthermore, C_L and $\sin\alpha$ are both non-decreasing in α. As a result,

$$-\frac{\varrho V_{\mathrm{t}} V_{\mathrm{d}}^2 (\sin\alpha - \sin\alpha_{\mathrm{d}}) \left(C_L - C_{L_{\mathrm{d}}} \right) \cos\alpha}{\cos\beta} \leq 0$$

Lastly, C_S and $\sin\beta$ have the same sign as β, which means $-\varrho V V_{\mathrm{d}}^2 C_S \sin\beta \leq 0$. But the term $-\frac{V_{\mathrm{d}} \sin^2\beta}{V} (\zeta_1 \cos\alpha + \zeta_3 \sin\alpha)$ is not guaranteed to be nonpositive. This term is however bounded since $|\zeta_1 \cos\alpha + \zeta_3 \sin\alpha| \leq 1$. Thus, for a sufficiently large airspeed, the sum of both terms is nonpositive. Hence, by restricting the stability analysis to a level set of the Lyapunov function defined to restrict the worst-case excursion in airspeed, one can verify that $\dot{\mathcal{H}}_{\mathrm{c}} \leq 0$, thereby showing that the desired equilibrium is stable. To show asymptotic stability, we use LaSalle's invariance principle.

LaSalle's principle states that trajectories which begin in a compact and positively invariant set Ω, where the Lyapunov conditions hold, converge to the largest invariant set M contained in the set $E = \{(\boldsymbol{h}, \boldsymbol{p}, \boldsymbol{\zeta}, \psi) \subset \Omega \mid \dot{\mathcal{H}}_{\mathrm{c}} = 0\}$. It can be easily shown that $\dot{\mathcal{H}}_{\mathrm{c}} = 0$ if and only if $\boldsymbol{\omega} = \mathbf{0}$, $V = V_{\mathrm{t}}$, $\alpha = \alpha_{\mathrm{d}}$, $\beta = 0$ and $\zeta_2 = 0$. Depending on the set Ω, however, there could be more than one state contained within M. To determine all possible states contained in M, one must consider the dynamics within the set E. Referring to equation (11), we find that

$$\mathbf{0} = k_\zeta \hat{\boldsymbol{\zeta}}_{\mathrm{d}} (\boldsymbol{\zeta} - \boldsymbol{\zeta}_{\mathrm{d}}) + \frac{k_\psi}{1 - \zeta_1^2} \begin{bmatrix} 0 \\ 0 \\ \zeta_3 \end{bmatrix} (\psi - \psi_{\mathrm{d}}) \tag{40}$$

Further investigation shows that the equation is satisfied if and only if $\boldsymbol{\zeta} = \boldsymbol{\zeta}_{\mathrm{d}}$ and $\psi = \psi_{\mathrm{d}}$. The equilibrium is therefore (locally) asymptotically stable. To estimate the basin of attraction, one may examine level sets of the Lyapunov function keeping in mind the requirement that the airspeed remain sufficiently high.

Remark 2. In applications where energy shaping is used to stabilize a port-Hamiltonian system, one typically shows that the closed-loop dynamics are Hamiltonian with respect to a control-modified Hamiltonian, and then proceeds with stability analysis. For the fixed-wing nonlinear flight control problem considered here, we were unable to obtain a coordinate transformation under which the closed-loop dynamics can be recognized as a Hamiltonian system. Doing so requires solving a system of PDEs whose solution is not intuitive, even when the functional form of the aerodynamic force coefficients is explicit. In our case, we consider a general class of aerodynamic force coefficients and show, in the proof of Theorem 1, that the function H_c is indeed a Lyapunov function. .

5 Simulation

To demonstrate the control law presented earlier, we simulate its performance using a flight dynamic model from the T-2 Generic Transport Model (GTM) presented by Grauer and Morelli [26]. The aerodynamic moment model is

$$\boldsymbol{\tau}_{\mathrm{a}} = -\frac{1}{2}\rho V^2 S L \boldsymbol{D}_{\omega}\boldsymbol{\omega}$$

with $\boldsymbol{D}_{\omega} = \mathrm{diag}(d_{\omega_1}, d_{\omega_2}, d_{\omega_3})$.

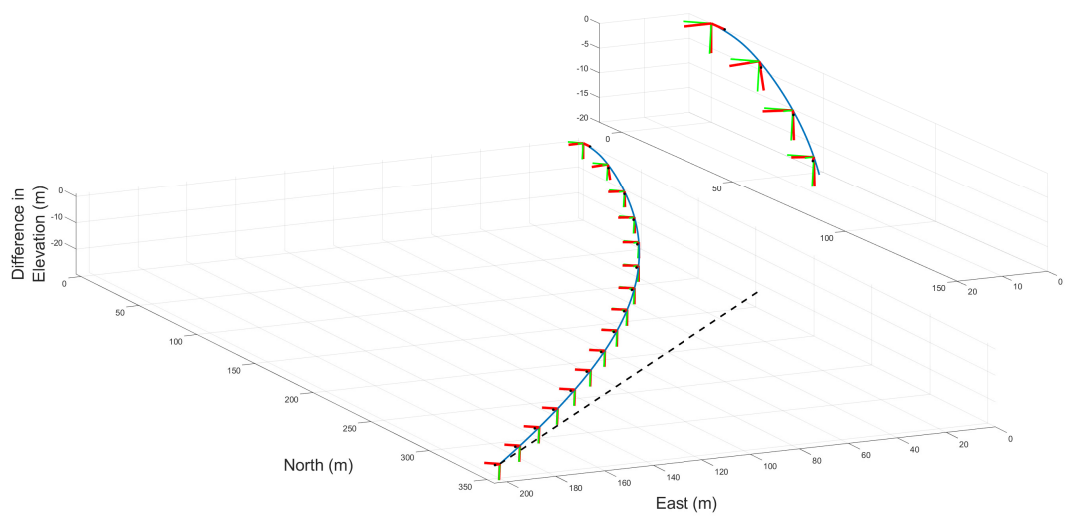

Figure 2: Desired velocity direction (dashed black) and actual path (solid blue). The initial position is the origin. Vehicle attitude is denoted at one second intervals by a red orthonormal triad; green triads denote desired attitude. Inset: Close-up of the initial closed-loop response.

In the simulation, the aircraft starts with an airspeed of 20 m/s and with initial values of zero for α and β. The desired motion corresponds to wings-level flight at an angle of attack of 10° with a zero climb angle and

a course angle of 45° (northeast). Initial values for state variables other than velocity were chosen randomly. The results shown in Figure 2 reflect the analytical stability results presented earlier, although the simulation model incorporates aerodynamic interactions which were ignored in the control design and analysis, such as aerodynamic force terms involving angular rates.

Figure 2 shows the vehicle's resultant trajectory (solid line) using the proposed controller subject to the previously stated initial conditions. The aircraft's orientation is indicated by a red orthogonal triad while its desired orientation at steady state is shown by a green orthogonal triad. The feedback controlled trajectory converges to the desired flight profile. Figure 4 shows the time history of rates and attitude variables as solid lines and the corresponding desired steady state values as dotted lines.

Additional simulations have been performed to explore the assumption that thrust is aligned with velocity. This assumption differs from the more common assumption that thrust is aligned with the longitudinal axis. While physical mechanisms are available to adjust the line of thrust, neither of these two assumptions is especially accurate for a generic aircraft with a fixed propulsor. In any case, to examine the sensitivity of the stability results to the thrust direction and magnitude, we include two sets of additional simulations – one set for which the commanded thrust magnitude is directed along the body-fixed $\boldsymbol{b}_1$ axis and another set where constant thrust is applied along $\boldsymbol{b}_1$. The time history of the Lyapunov function, as well as its rate of change, are shown in Figure 5. The non-negative Lyapunov function decreases monotonically for the original control, as it must do, and appears to do the same when the commanded thrust magnitude is directed along the longitudinal axis. This is not the case when using constant thrust, however, but the aircraft motion converges to the desired one in any case.

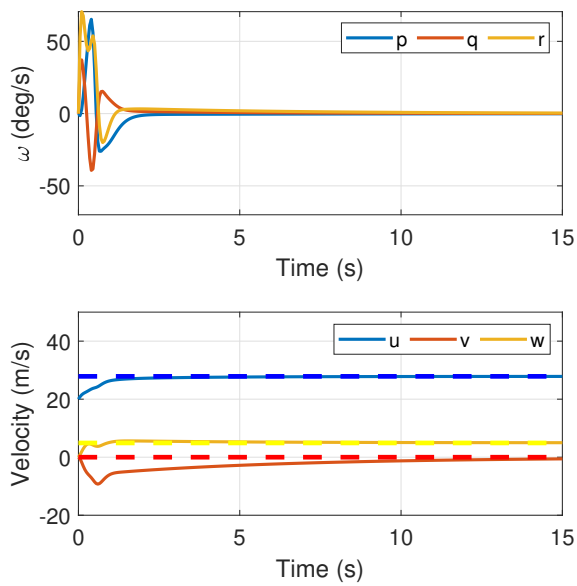

Figure 3: Desired (dashed) and actual (solid) both angular and translational velocity histories corresponding to Figure 2.

Additional simulations were conducted to study the controller's behavior in the presence of other types of model uncertainties. The model uncertainties considered can be categorized into two classes: uncertainties in inertia-related terms and uncertainties in the aerodynamic model. All the simulations begin with the initial state previously described and are prescribed the same desired steady state as above with a simulation time of 40 seconds. The simulations indicate that the closed-loop performance is robust to the uncertainties in the

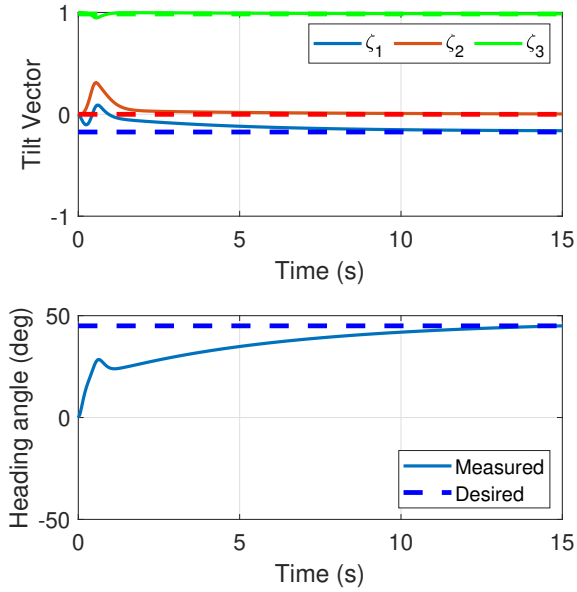

Figure 4: Desired (dashed) and actual (solid) attitude histories corresponding to Figure 2.

sense that the system remains stable and the state converges to a steady motion in the neighborhood of the desired motion. To quantify the effect of perturbations, an appropriate metric was defined. First, we define the time-averaged root mean squared (RMS) deviation, P of the velocity direction from the desired value for the perturbed flight dynamic model:

$$P = \frac{1}{T_{\mathrm{s}}} \int_0^{T_{\mathrm{s}}} \left(\frac{\mathbf{R}_{\mathbb{IB}}(t)\boldsymbol{p}(t)}{\|\boldsymbol{p}(t)\|} - \boldsymbol{i}_{\mathrm{d}} \right)^{\mathrm{T}} \left(\frac{\mathbf{R}_{\mathbb{IB}}(t)\boldsymbol{p}(t)}{\|\boldsymbol{p}(t)\|} - \boldsymbol{i}_{\mathrm{d}} \right) dt \tag{41}$$

where T_{s} is the total simulation time and $\boldsymbol{i}_{\mathrm{d}} = e^{-\chi_{\mathrm{d}}\hat{\boldsymbol{e}}_3} e^{-\gamma_{\mathrm{d}}\hat{\boldsymbol{e}}_2} \boldsymbol{e}_1$ is the desired inertial velocity direction. We define N similarly as the time-averaged RMS deviation of the velocity direction for the nominal plant. The error metric is taken as

$$E = \left| \frac{P - N}{N} \right| \tag{42}$$

5.1 Uncertainty in inertial parameters

For uncertainties in the inertial parameters, we consider perturbations to the mass matrix only. For each simulation, these perturbations are randomly generated, with a uniform distribution ranging between $\pm 10\%$ of each of their corresponding term's nominal value. All other parameters are kept the same as before. The controller is fed accurate traslational and rotational velocities, as well as position and attitude data, and computes the respective momenta, in addition to the required system inputs, using the nominal mass matrix. 1,000 numerical simulations of the closed-loop system were conducted under these conditions. Results indicate that the state remains within a neighborhood of the desired steady state, as shown by the histogram in Figure 6.

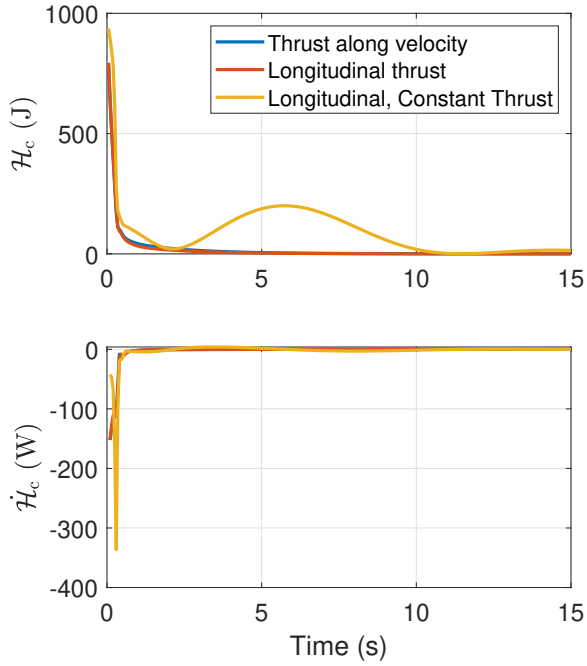

Figure 5: Lyapunov function and Lyapunov rate histories for different cases.

5.2 Uncertainty in aerodynamic model

The uncertainty in the aerodynamic model takes the form of perturbations to the aerodynamic coefficients. As before, the perturbations are generated at random in a uniform distribution ranging between $\pm 10\%$ of the corresponding term's nominal value. The aerodynamic model uncertainties that are considered fall in three categories: uncertainty in the aerodynamic force due to the translational velocity, uncertainty in the aerodynamic moment due to the angular velocity and uncertainty in the aerodynamic moment due to the translational velocity. The first two sources act on terms and quantities already accounted for in the simulation model. With regard to aerodynamic moments due to translational velocity, recall that these terms were omitted from consideration with the understanding that their effect should later be removed from the computed control moment. The concept is akin to feedback linearization, so it is especially important to assess the effect of uncertainty in these terms. For expedience, the coefficients are classified as being related to the angle of attack (α-dominant) or being related to the sideslip angle (β-dominant). Then, the coefficients of the same class are perturbed by the same randomly generated number. Like before, 1,000 numerical simulations of the closed-loop system were conducted under these conditions. As shown by the histogram in Figure 8, results show that the state remains within a neighborhood of the desired steady state.

The simulation results suggest the performance is more sensitive to perturbations in α-dominant terms than any other terms as shown in Figure 9.

5.3 Comparison to other controllers

To better understand the effectiveness of the controller compared to other approaches, we consider two alternative control design approaches, one linear and one nonlinear. Since the control law developed here involves static state feedback, we compare with other static state feedback methods. Thus, we do not con-

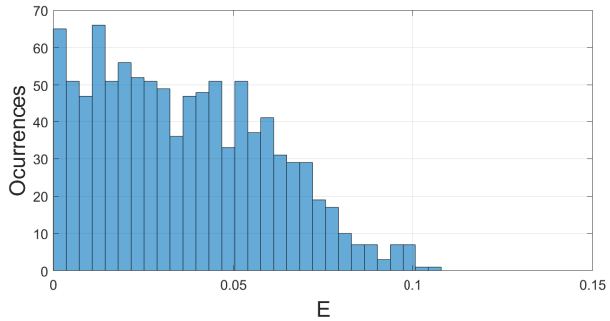

Figure 6: Histogram of E for 1000 simulations with uncertain inertia properties.

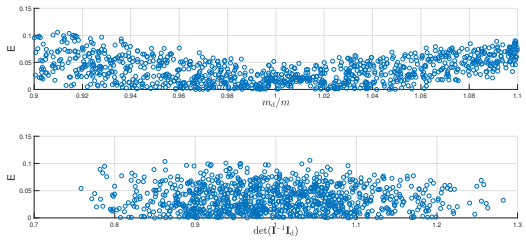

Figure 7: Controller performance versus uncertainty in the aircraft's mass (top) and inertia (bottom). The subscript "d" indicates terms with perturbations.

sider adaptive control or integral action. While dynamic state feedback can mitigate unwanted effects due to parameter uncertainty, for example, it also introduces additional complexity into the control system, with corresponding concerns about computation, integrator wind-up, etc. In any case, it is fairest to compare the proposed control method to other static feedback strategies.

To begin, an output feedback linear-quadratic regulator (LQR) was designed with a comparable control objective to that of the passivity-based controller. The output vector considered is $\boldsymbol{y}_{\mathrm{LQR}} = \left[\boldsymbol{h}^{\mathrm{T}}, \boldsymbol{p}^{\mathrm{T}}, \zeta_1, \psi\right]^{\mathrm{T}}$ and its desired value is $\boldsymbol{y}_{\mathrm{LQR_d}} = \left[\mathbf{0}, m\boldsymbol{v}_{\mathrm{d}}^{\mathrm{T}}, -\sin\alpha_{\mathrm{d}}, \psi_{\mathrm{d}}\right]^{\mathrm{T}}$. The control gains were computed using the linearized, nominal system. As before, the controller is subject to uncertainty analysis in the inertial parameters and the aerodynamic model. Each simulation begins with the same initial conditions as before and subject to the performance metric (41) and (42). One thousand numerical simulations of the closed-loop system were conducted for each type of uncertainty, once with the perturbed linearized dynamic model and another time with the nonlinear system model. The results in Figures 10-13 indicate that the performance of the LQR controller applied to the linearized dynamics is less sensitive to model parameter error than the performance of the proposed nonlinear controller applied to the nonlinear system model. When the LQR controller is applied to the nonlinear dynamic model, however, it performs significantly worse than the proposed controller. Figures 14-17 show a comparison between the two controllers' performance for the nonlinear dynamic model. In this comparison, the aircraft begins at the desired equilibrium profile as before and is tasked to modify its heading by 5 degrees. This control task is less aggressive to ensure that the LQR controller maintains control. The change in the control task affects the sensitivity results for both controllers. Because the denominator in the error metric (42), corresponding to the nominal motion, is much smaller for this less aggressive maneuver, the error metric values are larger in this scenario. In any case, the figures indicate that the LQR controller is much more sensitive to the given model uncertainties.

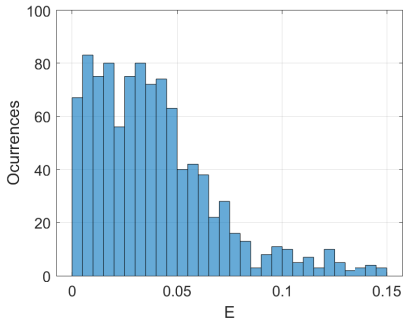

Figure 8: Histogram of E for 1000 simulations with uncertain aerodynamic parameters.

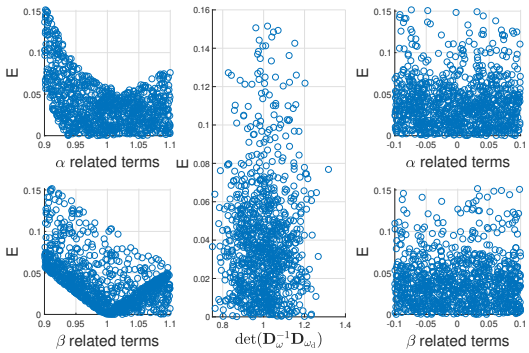

Figure 9: Controller performance, given uncertainty in the aerodynamic force (left), aerodynamic moment due to rotational velocity (middle), and aerodynamic moment due to translational velocity (right). The subscript "d" indicates the terms with perturbation.

In addition, a nonlinear controller was considered. The dynamic inversion controller described by Lane and Stengel [27] is chosen due to its popularity and ease of implementation. In line with the methodology detailed in the paper, a "control output" vector of the same dimensions as the input vector is taken. To present a fair comparison between the passivity-based and dynamic inversion controllers, the control input vector is selected to reflect quantities present in the control Hamiltonian in equation (23): $\bar{\boldsymbol{y}} = [\alpha - \alpha_{\mathrm{d}}, \beta, \zeta_1 + \sin\alpha_{\mathrm{d}}, \psi - \psi_{\mathrm{d}}]^{\mathrm{T}}$. Each element in the control output vector is differentiated, with respect to time, until at least one element of the control input vector appears. Hence, for each element of the output vector, $\bar{y}_i$, one obtains an equation of the form $\bar{y}_i^{(d_i)} = b_i + \boldsymbol{B}_i\boldsymbol{u}$, where the superscript (d_i) denotes the number d_i of time derivatives that are taken, b_i is the sum of all the terms that are independent of the input, and $\boldsymbol{B}_i$ is a row vector representing whether and how the various input components appear in the given derivative of $\bar{\boldsymbol{y}}_i$. Let $\boldsymbol{b}$ be the vector formed by concatenating all the b_i's and $\boldsymbol{B}$ be the matrix constructed by stacking all the $\boldsymbol{B}_i$'s. The inverse dynamics control law can be written as

$$\boldsymbol{u} = -\boldsymbol{B}^{-1}(\boldsymbol{b} + \boldsymbol{v}), \tag{43}$$

where $\boldsymbol{v} = \sum_{k=0}^{d-1} \boldsymbol{P}_k \bar{\boldsymbol{y}}^{(k)}$. Here, $\boldsymbol{P}_k$ is a set of preselected, constant matrices. For the sake of this comparison study, the set $\boldsymbol{P}_k$ is selected to achieve a performance similar to that of the passivity-based controller.

Initially, the uncertainty analysis was set up analogously to that of the passivity-based controller. Unfortunately, the inverse dynamics controller ran into situations where the $\boldsymbol{B}$ matrix became singular, indicating a loss of well-defined vector relative degree. To work around the issue, the initial condition was modified.

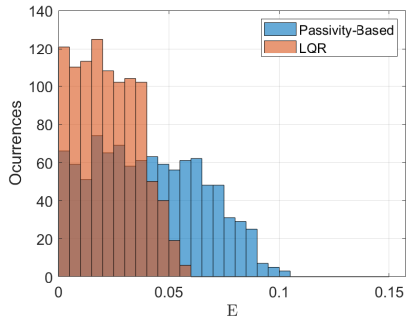

Figure 10: Histogram of E for 1000 simulations with uncertain inertia properties for an LQR controller applied to a linearized dynamic model compared to passivity-based control of the nonlinear dynamics.

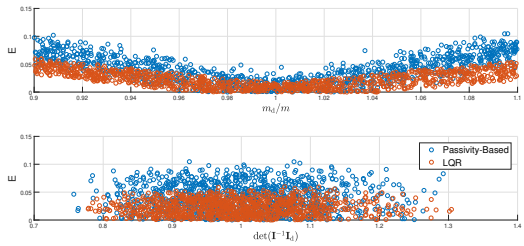

Figure 11: Comparison of the LQR controller's performance versus uncertainty in the aircraft's mass (top) and inertia (bottom) for the linearized dynamic model with the performance of the passivity-based controller for the nonlinear dynamics. The subscript "d" indicates the terms with perturbation.

Instead of starting out with zero roll, pitch and yaw, simulations began with a pitch and roll angle of 45°. The uncertainty analysis for the passivity-based controller was redone with the new initial conditions and the results are shown in Figures 18 and 19 for uncertainties in the inertial parameters and in Figures 20 and 21 for uncertainties in the aerodynamic parameters.

The results show comparable performance when considering uncertainties in inertia parameters. However, upon inspecting Figure 20, one may notice that the tail of the distribution pertaining to dynamic inversion is much longer than that for passivity-based control. This observation suggests that the proposed controller is more robust to uncertainties in the aerodynamic model.

6 Conclusion

This paper presents a nonlinear, energy-based control design for a small, fixed wing aircraft which stabilizes the aircraft to wings-level flight at a commanded velocity, characterized by a desired speed, course, and climb angle. The control law requires knowledge of some aerodynamic parameters, but the stability analysis uses very general assumptions about the aerodynamic forces and moments.

By recognizing a special structure of the aerodynamics, it is possible to cast the aircraft equations of motion as a port-Hamiltonian system. Thus, one may leverage the system's passivity properties to design a nonlinear, energy-based control strategy. A Lyapunov function candidate was constructed by modifying the storage function; the stability proof relies on exploiting the structure of the port-Hamiltonian system model.

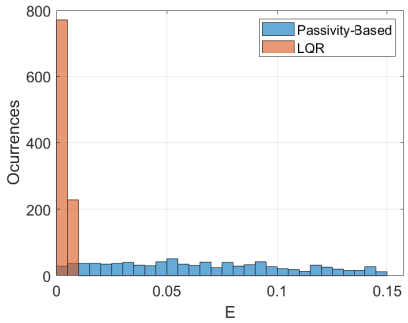

Figure 12: Histogram of E for 1000 simulations with uncertain aerodynamic parameters for an LQR controller applied to the linearized dynamics and passivity-based control of the nonlinear dynamics.

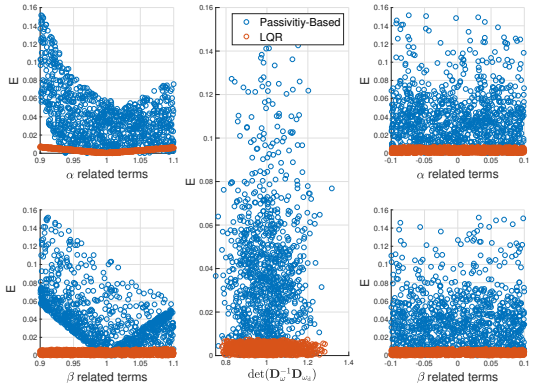

Figure 13: Comparison of the LQR controller's performance versus uncertainty in the aerodynamic force (left), aerodynamic moment due to rotational velocity (middle), and aerodynamic moment due to translational velocity (right) for the linearized dynamic model with the performance of the passivity-based controller for the nonlinear dynamics. The subscript "d" indicates the terms with perturbation.

Simulations illustrate that the control law is robust to model parameter uncertainty and that its performance compares favorably with two other static state feedback methods, the linear-quadratic regulator and dynamic inversion.

Future work involves adapting the control law presented here to stabilize a time-varying desired velocity, which is a precursor for curvilinear path-following.

Acknowledgments. The authors gratefully acknowledge our fruitful conversations with Dr. Francis Valentinis. This work was supported in part by the National Science Foundation under Grant CNS-1650465 and in part by the National Aeronautics and Space Administration (NASA) under Grant 80NSSC20M0162.

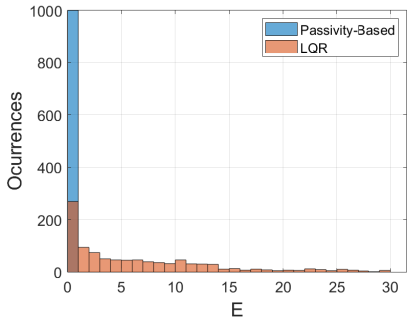

Figure 14: Histogram of E for 1000 simulations with uncertain inertia properties comparing the performance of the proposed controller with an LQR control law applied to the nonlinear dynamics.

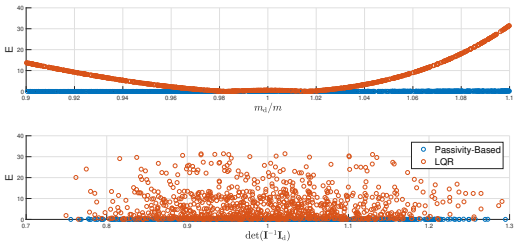

Figure 15: Performance comparison of the LQR and passivity-based controllers, when applied to the nonlinear system model, given uncertainty in the aircraft's mass (top) and inertia (bottom). The subscript "d" indicates the terms with perturbation.

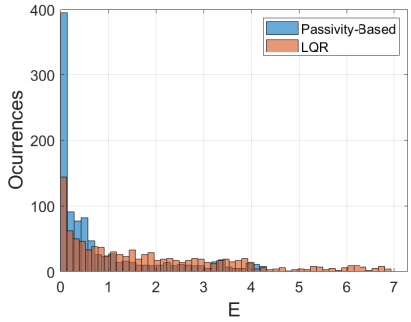

Figure 16: Histogram of E for 1000 simulations with uncertain aerodynamic parameters comparing the performance of the proposed controller with an LQR control law applied to the nonlinear dynamics.

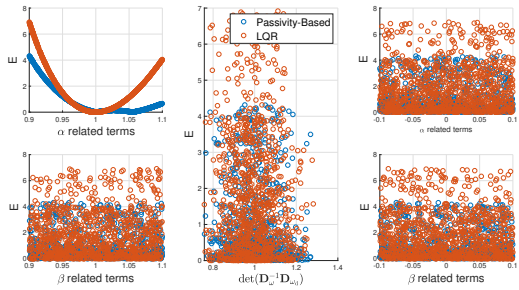

Figure 17: Performance comparison of the LQR and passivity-based controllers, when applied to the nonlinear system model, given uncertainty in the aerodynamic force (left), aerodynamic moment due to rotational velocity (middle) and aerodynamic moment due to translational velocity (right). The subscript "d" indicates the terms with perturbation.

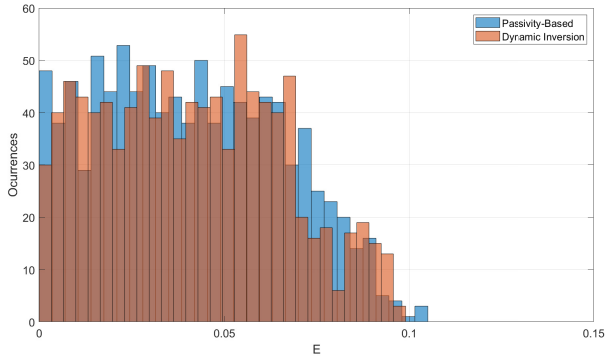

Figure 18: Histogram comparing performance of the passivity-based and dynamic inversion controllers for 1000 simulations with uncertain inertia parameters.

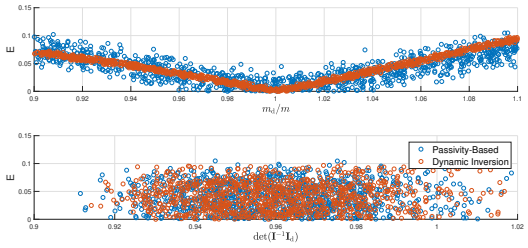

Figure 19: Performance comparison of the passivity-based and dynamic inversion controllers, given uncertainty in the aircraft's mass (top) and inertia (bottom). The subscript "d" indicates the terms with perturbation.

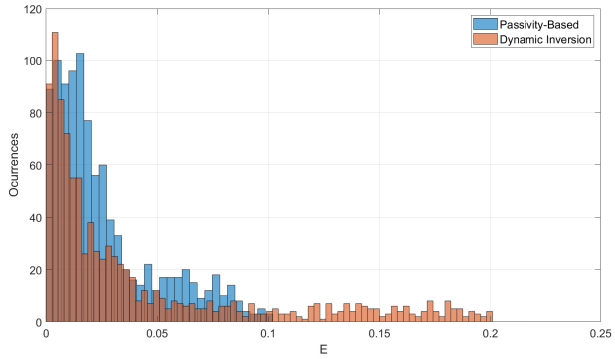

Figure 20: Histogram comparing performance of the passivity-based and dynamic inversion controllers for 1000 simulations with uncertain aerodynamic parameters.

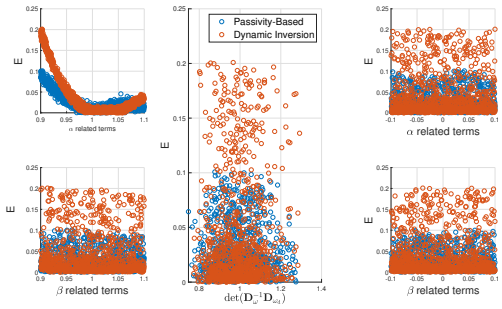

Figure 21: Performance comparison of the passivity-based and dynamic inversion controllers, given uncertainty in the aerodynamic force (left), aerodynamic moment due to rotational velocity (middle), and aerodynamic moment due to translational velocity (right). The subscript "d" indicates the terms with perturbation.

References

[1] S. A. Snell, D. F. Enns, and Jr. W. L. Garrard. Nonlinear inversion flight control for a supermaneuverable aircraft. *AIAA Journal of Guidance, Control, and Dynamics*, 15(4):976–984, July-August 1992. 1

[2] H. K. Khalil. *Nonlinear Systems*, volume Upper Saddle River, NJ. Prentice-Hall, second edition, 1996. 1

[3] S. Sastry. *Nonlinear Systems: Analysis, Stability, and Control*. Springer, New York, NY, 2013. 1

[4] N. Hovakimyan and C. Cao. L_1 *Adaptive Control Theory: Guaranteed Robustness with Fast Adaptation*. Society for Industrial and Applied Mathematics, Philadelphia, PA, 2010. 1

[5] M. Krstic, I. Kanellakopoulos, and P. V. Kokotovic. *Nonlinear and Adaptive Control Design*. Wiley, Hoboken, NJ, 1995. 1

[6] K. J. Åström and B. Wittenmark. *Adaptive Control*. Courier Corporation, North Chelmsford, MA, 2013. 1

[7] A. van der Schaft. *L2-gain and passivity techniques in nonlinear control*, volume 2. Springer, 2000. 1, 3

[8] R. Ortega and E. Garcia-Canseco. Interconnection and damping assignment passivity-based control: A survey. *European Journal of control*, 10(5):432–450, 2004. 2

[9] R. Ortega, A. van der Schaft, B. Maschke, and G. Escobar. Interconnection and damping assignment passivity-based control of port-controlled hamiltonian systems. *Automatica*, 38(4):585–596, 2002. 2

[10] H. Gonzalez, M. A. Duarte-Mermoud, I. Pelissier, J. C. Travieso-Torres, and R. Ortega. A novel induction motor control scheme using ida-pbc. *Journal of Control Theory and Applications*, 6(1):59–68, 2008. 2

[11] L. C. Neves, G. V. Paim, I. Queinnec, U. F. Moreno, and E. R. De Pieri. Passivity and power based control of a robot with parallel architecture. *IFAC Proceedings Volumes*, 44(1):14608–14613, 2011. 2

[12] M. Ryalat and D. S. Laila. A simplified ida-pbc design for underactuated mechanical systems with applications. *European Journal of Control*, 27:1–16, 2016. 2

[13] V. Santibanez, R. Kelly, and J. Sandoval. Control of the inertia wheel pendulum by bounded torques. In *Proceedings of the 44th IEEE Conference on Decision and Control*, pages 8266–8270. IEEE, 2005. 2

[14] J. A. Acosta, M. I. Sanchez, and A. Ollero. Robust control of underactuated aerial manipulators via ida-pbc. In *53rd IEEE Conference on Decision and Control*, pages 673–678. IEEE, 2014. 2

[15] M. E. Guerrero, D. A. Mercado, R. Lozano, and C. D. García. IDA-PBC methodology for a quadrotor uav transporting a cable-suspended payload. In *2015 International Conference on Unmanned Aircraft Systems (ICUAS)*, pages 470–476. IEEE, 2015. 2

[16] B. Yüksel, C. Secchi, H. H. Bülthoff, and A. Franchi. Reshaping the physical properties of a quadrotor through ida-pbc and its application to aerial physical interaction. In *2014 IEEE International Conference on Robotics and Automation (ICRA)*, pages 6258–6265. IEEE, 2014. 2

[17] A. Y. Mersha, R. Carloni, and S. Stramigioli. Port-based modeling and control of underactuated aerial vehicles. In *2011 IEEE International Conference on Robotics and Automation*, pages 14–19. IEEE, 2011. 2

[18] L. E. Muñoz, O. Santos, P. Castillo, and I. Fantoni. Energy-based nonlinear control for a quadrotor rotorcraft. In *2013 American Control Conference*, pages 1177–1182. IEEE, 2013. 2

[19] C. A. Woolsey. Cross-track control of a slender, underactuated auv using potential shaping. *Ocean Engineering*, 36(1):82–91, 2009. 2

[20] J.-M. Fahmi and C. Woolsey. Directional stabilization of a fixed-wing aircraft using potential shaping. In *Atmospheric Flight Mechanics Conference*, Atlanta, GA, June 2018. 2

[21] Francis Valentinis, Alejandro Donaire, and Tristan Perez. Energy-based motion control of a slender hull unmanned underwater vehicle. *Ocean Engineering*, 104:604–616, 2015. 2

[22] F. Valentinis, A. Donaire, and T. Perez. Energy-based guidance of an underactuated unmanned underwater vehicle on a helical trajectory. *Control Engineering Practice*, 44:138–156, 2015. 2

[23] F. Valentinis and C. Woolsey. Nonlinear control of a subscale submarine in emergency ascent. *Ocean Engineering*, 171:646–662, 2019. 2

[24] K. Fujimoto, K. Sakurama, and T. Sugie. Trajectory tracking control of port-controlled Hamiltonian systems via generalized canonical transformations. *Automatica*, 39(12):2059–2069, 2003. 2, 6

[25] T. Battista, S. Jung, C. A. Woolsey, and E. G. Paterson. An energy-casimir approach to underwater vehicle depth and heading regulation in short crested waves. In *Proc. IEEE Conference on Control Technology and Applications*, Kohala Coast, Hawai'i, USA, August 2017. 4

[26] J. A. Grauer and E. A. Morelli. A generic nonlinear aerodynamic model for aircraft. In *Proc. AIAA Atmospheric Flight Mechanics Conference*, National Harbor, MD, USA, August 2014. 12

[27] Stephen H Lane and Robert F Stengel. Flight control design using non-linear inverse dynamics. *Automatica*, 24(4):471–483, 1988. 17